JACS
JOURNAL OF THE AMERICAN CHEMICAL SOCIETY
Cite This: J. Am. Chem. Soc. 2019, 141, 14581−14592
Article
pubs.acs.org/JACS

Ultrafast Proton Transport between a Hydroxy Acid and a Nitrogen Base along Solvent Bridges Governed by the Hydroxide/Methoxide Transfer Mechanism

Maria Ekimova,[†] Felix Hoffmann,[‡] Gül Bekçioğlu-Neff,[‡] Aidan Rafferty,[†] Oleg Kornilov,[†] Erik T. J. Nibbering,*[,†] and Daniel Sebastiani*[,‡]

[†]Max Born Institut für Nichtlineare Optik und Kurzzeitspektroskopie, Max Born Str. 2A, 12489 Berlin, Germany
[‡]Institut für Chemie, Martin-Luther-Universität Halle-Wittenberg, Von-Danckelmann-Platz 4, 06120 Halle, Saale, Germany

Supporting Information

ABSTRACT: Aqueous proton transport plays a key role in acid−base neutralization and energy transport through biological membranes and hydrogen fuel cells. Extensive experimental and theoretical studies have resulted in a highly detailed elucidation of one of the underlying microscopic mechanisms for aqueous excess proton transport, known as the von Grotthuss mechanism, involving different hydrated proton configurations with associated high fluxional structural dynamics. Hydroxide transport, with approximately 2-fold-lower bulk diffusion rates compared to those of excess protons, has received much less attention. We present femtosecond UV/IR pump−probe experiments and ab initio molecular dynamics simulations of different proton transport pathways of bifunctional photoacid 7-hydroxyquinoline (7HQ) in water/methanol mixtures. For 7HQ solvent-dependent photoacidity, free-energy−reactivity correlation behavior and quantum mechanics/molecular mechanics (QM/MM) trajectories point to a dominant OH^-/CH_3O^- transport pathway for all water/methanol mixing ratios investigated. Our joint ultrafast infrared spectroscopic and ab initio molecular dynamics study provides conclusive evidence for the hydrolysis/methanolysis acid−base neutralization pathway, as formulated by Manfred Eigen half a century ago. Our findings on the distinctly different acid−base reactivities for aromatic hydroxyl and aromatic nitrogen functionalities suggest the usefulness of further exploration of these free-energy−reactivity correlations as a function of solvent polarity. Ultimately the determination of solvent-dependent acidities will contribute to a better understanding of proton-transport mechanisms at weakly polar surfaces and near polar or ionic regions in transmembrane proton pump proteins or hydrogen fuel cell materials.

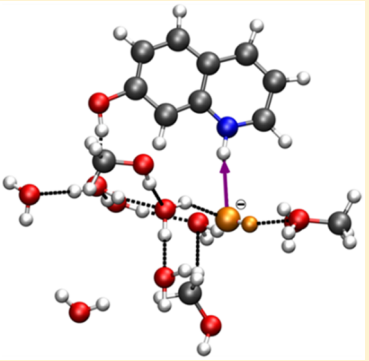

1. INTRODUCTION

Aqueous acid−base neutralization involves a proton exchange with the strong involvement of water solvent molecules. The current understanding of proton exchange between Brønsted acids and Brønsted bases originated from seminal studies by Eigen[1] and Weller[2] more than half a century ago. The general kinetic scheme has been described in Eigen's review of the field.[3] According to the scheme, the proton transfer converting the acid−base reactant pair to its conjugate acid−conjugate base product pair is considered to follow either a concerted or sequential pathway (Figure 1a). In the sequential (proton-hopping) case, two possible directions for proton transport can in principle occur: either a forward excess proton transfer from acid via intermediate hydrated protons to the accepting base (protolysis pathway) or an inverse proton-defect transport (hydrolysis pathway) where the base extracts a proton from the solvent, generating hydrated hydroxide anions that ultimately react with the acid.[4,5] A third pathway involves a direct proton exchange between acid and base, with an underlying concerted proton transfer mechanism. Which proton transfer pathway prevails depends on the relative reaction rates of the individual proton transfer steps. The relevance of proton transport in cases as diverse as hydrogen fuel cells and biochemical environments, including transmembrane protein channels,[6−9] necessitates a further exploration of the underlying proton transport mechanisms for conditions clearly distinct from those of bulk water (i.e., for lower-polarity solvent media and possible crucial roles of hydrophobic alkyl- and hydrophilic alcohol functionalities).

Experimental and theoretical results point to a water-mediated proton transfer mechanism on ultrafast time scales between aromatic alcohols and carboxylate bases.[10−15] A limited number of intermediate water molecules connecting these acid and base molecules facilitate the protolysis pathway through a hydrogen-bonded "water bridge" or "water wire". These findings can be compared to theoretical studies on proton transport in bulk water, where the transport mechanism of the excess proton has been intensively explored.[16−18] It has been found that different conformations of hydrated protons play a key role in the sequential von Grotthuss-type proton hopping mechanism, with Eigen-type (hydronium, H_3O^+) or

Received: March 31, 2019
Published: August 26, 2019

DOI: 10.1021/jacs.9b03471
J. Am. Chem. Soc. 2019, 141, 14581−14592

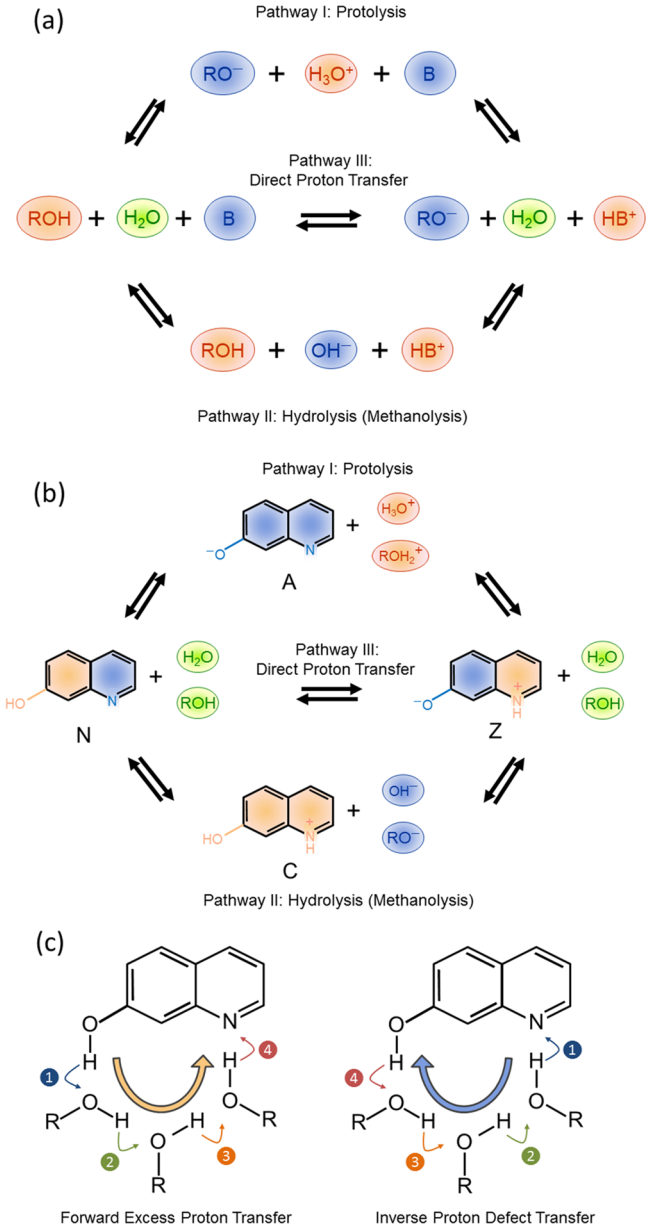

Figure 1. (a) Eigen's reaction scheme. (b) Eigen's scheme adapted to 7HQ. (c) Forward excess proton transfer vs inverse proton defect transfer with the sequence of proton transfer events along the solvent bridge for 7HQ.

Zundel-type ($H_5O_2^+$) hydrated protons often found to occur at distinct phases of the elementary proton hopping events.[19−22] Hydroxide (OH^-) transport has been considered only in a small number of ab initio molecular dynamics studies,[23−25] where for OH^- transport in bulk water two different hydrated forms of OH^- have been found. These studies found OH^- transfer to occur by either 4- or 5-fold hydrated configurations, with OH^- donating one and accepting three or four hydrogen bonds to first solvation shell water molecules, respectively.

In this report, we present the results of a joint experimental and theoretical study of proton transfer between the proton-donating OH group of an acid and the proton-accepting aromatic N-moiety of a base. To avoid a possible variation of the distance between the acid and base, thus maintaining a well-defined number of solvent molecules forming the solvent bridge, we use a so-called bifunctional photoacid,[26] 7-hydroxyquinoline (7HQ)[27−32] (Figure 1b). This bifunctional compound has both the photoacid properties of 2-naphthol and the photobase properties of quinoline. Excitation to the first electronically excited state results in a pK_a jump from 8.67 to around 0.4 for the OH group and from 5.64 to around 11.1 for the N side (Table 1). As a result, both the acidity of the OH group and the basicity of the N-group strongly increase, initiating a net proton transfer from the neutral (N*) to the zwitterionic (Z*) form with a time constant of ∼37 ps in water[28] and 170 ps in methanol.[29] In a previous study, we characterized 7HQ dissolved in deuterated methanol (CD_3OD)[33] and found the IR-active fingerprint patterns of N*, Z*, and intermediate A* or C* that are expected to occur when the reaction proceeds through a forward or an inverse proton transfer pathway, respectively (Figure 1c). We have assigned the IR-active fingerprint modes measured for tautomers N* and Z* and charged species A* and C* with quantum chemical calculations using time-dependent density functional theory.

Clearly the results obtained on the different tautomers and charged species of 7HQ are not sufficient to draw decisive conclusions on the following questions: (1) Are there distinct changes when going from methanol to water solution in terms of reaction rates, and if affirmative, can particular trends be specified? (2) Would a change from methanol to water facilitate the observation of possible intermediates? (3) If the results of ultrafast UV/IR pump−probe experiments are necessarily ensemble-averaged, then would state-of-the-art ab initio molecular dynamics simulations be sufficient to provide key insight into the underlying microscopic mechanisms of the

Table 1. Comparison of Previously Reported Time Constants Obtained from Ultrafast Spectroscopic Measurements on 7HQ and Derived Values for $\Delta pK_a = pK_a(\text{Donor}) - pK_a(\text{Protonated Acceptor})$

		CD_3OD			CH_3OH			H_2O		
equilibrium	functionality	time constant τ (ps)[a]	$-\log_{10}[k_r]$	ΔpK_a	time constant τ (ps)[b]	$-\log_{10}[k_r]$	ΔpK_a	time constant τ (ps)[c]	$-\log_{10}[k_r]$	ΔpK_a
C* + ROH ⇆ Z* + ROH_2^+	2-naphthol	160	9.80	1.0	114[d]			18	10.74	−1.0
N* + ROH ⇆ C* + RO^-	1-quinolinium	320	9.49	1.4	170	9.77	1.0	37	10.43	−0.25
N* + ROH ⇆ A* + ROH_2^+	2-naphthol									
A* + ROH ⇆ Z* + RO^-	1-quinolinium	600	9.22	1.75	428[d]			180	9.74	1.0

[a]Reference 33 from femtosecond UV/IR measurements. [b]Reference 29 from time-correlated single photon counting (TCSPC) measurements. [c]Reference 28 from TCSPC measurements. [d]Assuming a regular H/D kinetic isotope effect.

DOI: 10.1021/jacs.9b03471
J. Am. Chem. Soc. 2019, 141, 14581−14592

proton exchange? (4) Ultimately, is it possible to determine which reaction pathway of Figure 1b dominates the proton exchange dynamics. To answer these questions, we follow in this work the conversion of N* → Z* in real time for different water/methanol mixtures, further exploring the N* → Z* conversion kinetics with ultrafast UV/IR pump−probe spectroscopy. We characterize the reaction rates as a function of the X_{H_2O}:X_{CH_3OH} molar fraction ratio and look for the possible presence of transient species. To substantiate the observed reaction rates, we derive the differences in acidity of reactants and products and possible intermediates through the respective pK_a/pK_a* values using well-established free-energy reactivity correlations.[12,34−37] We conclude that for ensemble-averaged population kinetics upon photoexcitation of 7HQ, the proton transfer follows general rules for acidities when going from methanol to water. To further substantiate our findings that the proton transfer pathway through a sequential hydroxide/methoxide transport occurs for all X_{H_2O}:X_{CH_3OH} molar fraction ratios, we use quantum mechanics/molecular mechanics (QM/MM) molecular dynamics simulations applied to the S_1 state of 7HQ using time-dependent density functional theory (TD-DFT) calculations. We infer that the primary event of proton transfer for 7HQ involves a proton abstraction from the nearest solvent molecule to the quinoline N-side. Our combined experimental and theoretical results demonstrate that the hydrolysis/methanolysis pathway of acid−base neutralization through a water/methanol bridge consisting of three solvent molecules is the dominant pathway. Our results on the 7HQ model system have direct relevance not only for proton transport in water-rich solutions but also for less polar water-poor media, which are ubiquitous in the important cases of proton transport channels in transmembrane proteins or ion exchange regions within hydrogen fuel cells.

2. RESULTS AND DISCUSSION

2.1. Femtosecond UV/IR Pump−Probe Results. In Figure 2, we show the absorption and fluorescence spectra of 7HQ in water/methanol mixtures. The gradual shift in equilibrium constants with increased water fraction leads to a pronounced change in the relative populations of N and Z, and N* and Z*, in the S_0 and S_1 states, respectively. Femtosecond pump pulses tuned to 340 nm lead to the electronic excitation of 7HQ from the S_0 state of N to the S_1 state of the N* tautomer.

We have measured the transient response of the vibrational marker modes of 7HQ in the IR-active fingerprint spectral region between 1400 and 1550 cm^{-1}. In a previous publication,[33] we have reported on the distinct vibrational patterns for different charged species N*, C*, A*, and Z* dissolved in neat CD_3OD. We have used deuterated methanol as a solvent to facilitate direct access to the most important vibrational marker modes in this spectral region, which for normal methanol, CH_3OH, would be inaccessible under our experimental conditions. We have concluded that the deuteron transfer process occurs from N* to Z* with a 330 ps time constant. Figure 3a shows our transient IR-absorption spectra, with basic features similar for all water/methanol mixtures studied (i.e., for the X_{D_2O}:X_{CD_3OD} molar ratio ranging from 0.0:1.0 to 0.7:0.3). Indeed, we identify the N* marker mode located at 1475 cm^{-1} and the Z* marker mode at 1440 cm^{-1} to let us observe a profound increase in overall conversion rates from N* to Z* with increasing water content (Figure 3b). For

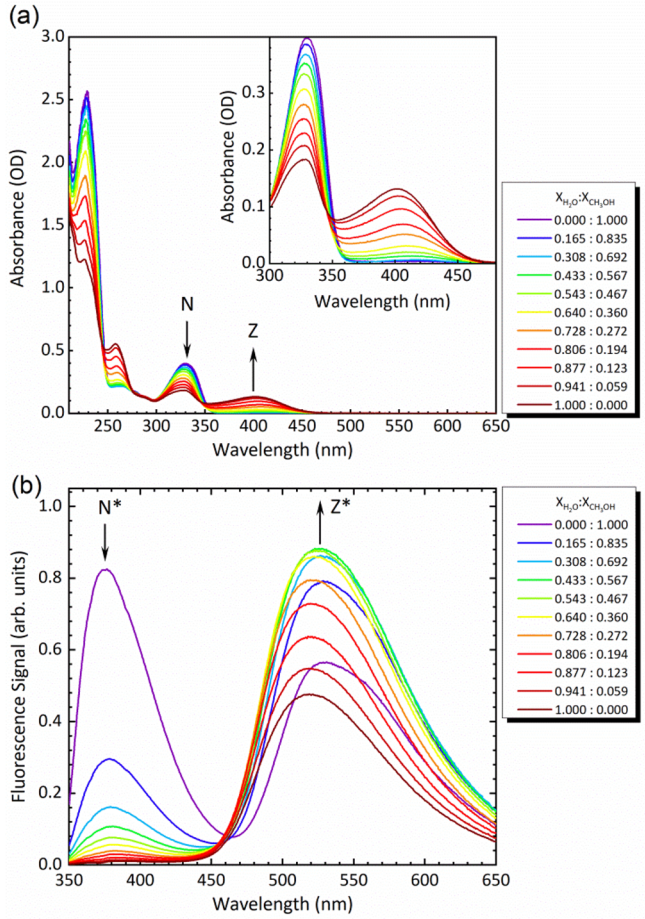

Figure 2. (a) Absorption and (b) emission spectra recorded for 7HQ in water/methanol mixtures with molar fractions X_{H_2O}:X_{CH_3OH} as indicated. The emission spectra, measured with a 330 nm excitation wavelength, reflect both the solvent-mixture-dependent chemical speciation of N and Z and a solvent-dependent fluorescence quantum yield.

all water/methanol solvent mixtures, the time scale of the decay of the N* population is equal to the rise of the Z* population. We have not observed significant spectral features indicative of transient population buildup of either the C* or A* species upon increased molar fraction of water. From these results, we conclude that the underlying proton transport mechanisms for 7HQ in water/methanol mixtures must be similar to those in neat methanol, up to the highest water molar fraction investigated here. An in-depth kinetic analysis of the transient IR spectra can be found in the Supporting Information. We summarize our findings of this kinetic analysis in Table 2 and compare the obtained time constant values with those previously reported. Apart from a fast, broad, spectrally featureless component (that occurs on a time scale of up to a few picoseconds) that may be caused by multiphoton/cross-phase modulation effects in the solvent and hydrogen bond rearrangements around the solute,[13,38−40] we note here that the population decay of N* follows the same temporal behavior on a time scale of hundreds of picoseconds as the population rise of Z* (i.e., no significant transient population of C* has been detected). This may suggest that either direct "concerted" proton transfer pathway III describes the proton exchange or that the first step in proton abstraction to or from the solvent is the rate-determining step. From our previous

DOI: 10.1021/jacs.9b03471
J. Am. Chem. Soc. 2019, 141, 14581−14592

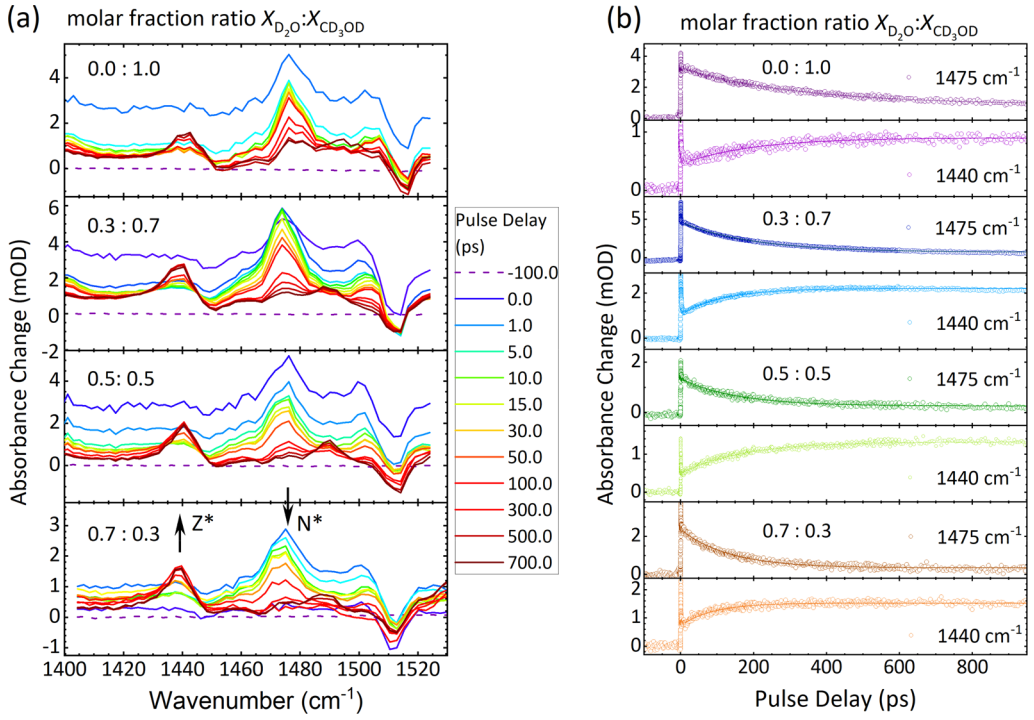

Figure 3. (a) Transient UV/IR spectra measured on 7HQ dissolved in D_2O/CD_3OD mixtures. (b) Population kinetics of the N* and Z* species, as measured through the 1475 and 1440 cm^{-1} marker bands, respectively.

Table 2. Free-Energy Reactivity Results Obtained on 7HQ in Deuterated Water/Methanol Mixtures

				pathway I		pathway II	
X_{D_2O}:X_{CD_3OD}	N* decay time constant (ps)	$-\log_{10}[k_r]$	ΔpK_a	calculated pK_a (N* species)	pK_a (solvent species D_3O^+ or $CD_3OD_2^+$)	pK_a (solvent species D_2O or CD_3OD)	calculated pK_a (C* species)
0.0:1.0	361	9.44	1.40	1.4	0.0	17.5	16.1
0.3:0.7	180	9.74	1.00	1.0	0.0	15.4	14.4
0.5:0.5	158	9.80	0.86	0.9	0.0	15.0	14.1
0.7:0.3	110	9.96	0.65	0.7	0.0	15.0	14.3
1.0:0.0	51[a,b]	10.28	0.0	0.0	0.0	15.0	15.0

[a]Reference 28 from TCSPC measurements. [b]Assuming the regular H/D kinetic isotope effect.

study, we determined a time constant of 320 ps for the N* → Z* conversion in deuterated methanol while the C* → Z* reaction occurs with a time constant of 160 ps.[33] This would imply a transient population build-up for C* of only 25% of the initially excited population for N*. However, it can be argued that the C* → Z* conversion will be much faster because the last step will be a neutralization reaction, C* + CD_3O^- → Z* + CD_3OD, rather than a deuteron donation to the solvent, C* + CD_3OD → Z* + $CD_3OD_2^+$. The results presented here suggest that this explanation holds for water/methanol mixtures.

2.2. Free-Energy Reactivity Analysis. To understand our observations we first discuss the reactivity of acids and bases as a function of the solvent medium. Typically, acidities in the condensed phase are quantified with pK_a values (i.e., $-\log_{10} K_a$, with $K_a = [B][H^+]/[HB^+]$, where "H^+" is a common indicator of the solvated proton species present in the particular solvent used and B is the conjugate base of acid HB), for the water solvent. Empirical data in other solvents (such as methanol, dimethyl sulfoxide, and acetonitrile as well as for particular solvent mixtures) now have been gathered, and solvent-dependent acidity relationships have been reported. In particular, a comparison of pK_a values of particular types of acids in water to those in methanol has shown that a strong variation occurs for phenol-type acids, but a significantly smaller solvent dependence happens for protonated nitrogen bases[41−43]

$$pK_a(CH_3OH) = m pK_a(H_2O) + c \quad (1)$$

where for phenols $m = 1.08$ and $c = 3.66$ and for protonated nitrogen bases $m = 1.02$ and $c = 0.72$. Hence, for phenol-type compounds the pK_a value is observed to increase by ∼3.5 to 4 units when going from H_2O to CH_3OH as a solvent, whereas for protonated nitrogen bases (amines, anilines, and N-heterocycles such as pyridines) the pK_a value increases only by about 0.5 to 1 unit.

Photoacid research has matured to a general understanding that the photoacidity effect results from an increase in acidity upon electronic excitation (i.e., $pK_a^* = pK_a(S_1)$ decreases by ∼6 to 7 units compared to the electronic ground state $pK_a(S_0)$ value for aromatic alcohols (phenols, naphthols, and hydroxypyrenes)). A large number of time-resolved fluorescence measurements, femtosecond UV/vis, and UV/IR pump−probe experiments have led to the conclusion that a free-energy−reactivity correlation of photoacids connects the thermodynamic quantities of acidity in the electronic excited

DOI: 10.1021/jacs.9b03471
J. Am. Chem. Soc. 2019, 141, 14581−14592

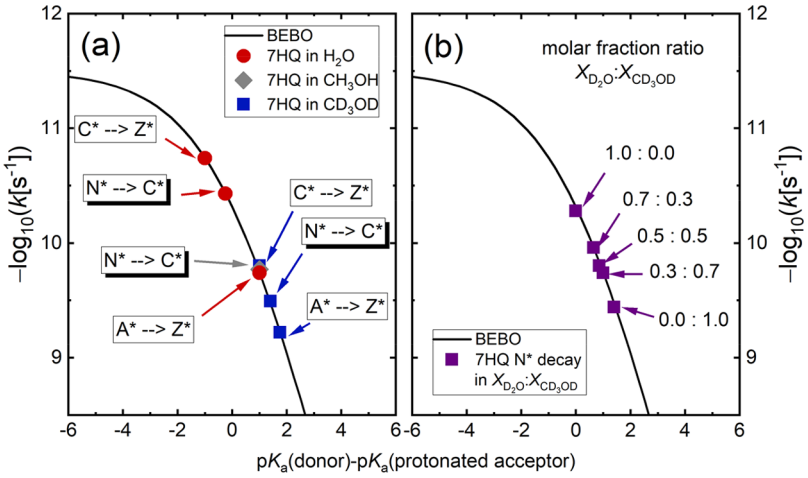

Figure 4. Free-energy−reactivity correlation of the different charged forms of photoexcited 7HQ in (a) H_2O, CH_3OH, or CD_3OD and (b) D_2O/CD_3OD mixtures. The Marcus bond energy bond order (BEBO) relationship is shown as a solid line.

state (i.e., pK_a* values) to proton transfer reaction rates. This free-energy−reactivity correlation holds for photoacid dissociation to the solvent water, proton abstraction from the solvent water by a photobase, and photoacid−base neutralization in aqueous solution and has even been shown to hold for the proton transfer of photoacids in methanol solution.[12,34−37,44,45]

The free-energy−reactivity correlation can be rationalized in terms of Marcus theory adapted to the case of proton transfer,[46] where solvent reorganization plays a dominant role, or by use of the bond-energy bond-order (BEBO) model[47] for proton transfer along a pre-existing hydrogen bond, which is valid for the opposite extreme condition reminiscent of nonadiabatic electron-transfer reactions. In the free-energy (ΔG_a) and accordingly ΔpK_a parameter value range relevant here (i.e., in the endothermic branch of the proton transfer reactions), these two descriptions lead to similar results. We summarize here only the main equations following the BEBO model. In the free-energy relationship

$$k_r = k^* \exp(-\Delta G_a/RT) \quad (2)$$

where k_r is the first-order rate constant and $(k^*)^{-1}$ is the frequency factor of this type of reaction, R is the gas constant, and T is the absolute temperature. We have set the parameter value for $(k^*)^{-1} = 10^{12}$ s^{-1} as found to be the most appropriate for numerous photoacid dissociation and photoacid−base neutralization reactions in protic solvents.[12,34−37,44,45] This is relatively slow compared to the inertial and librational motions in protic solvents water and methanol, which have about an order of magnitude shorter intrinsic time scales. The effective activation energy of the proton transfer reaction, ΔG_a, has been estimated using the Marcus BEBO equation:[48]

$$\Delta G_a = \frac{\Delta G^\circ}{2} + \Delta G_o^{\#} + \frac{\Delta G_o^{\#} \ln\left(\cosh\left[\frac{\Delta G^\circ \ln 2}{2\Delta G_o^{\#}}\right]\right)}{\ln 2} \quad (3)$$

Here $\Delta G_o^{\#}$ is the solvent-dependent activation energy of the charge-exchange reaction when the total free-energy change is ΔG° in the proton transfer reaction is equal to zero.

$$\Delta G^\circ = RT \ln 10\, \Delta pK_a$$

In principle, 7HQ can exhibit acid−base reactivity as an aromatic alcohol (through its 2-naphthol functionality) and as a protonated nitrogen base (through its quinolinium functionality). Free-energy−reactivity correlations can be used to derive an unknown pK_a value of one of the acids/conjugate acids of bases in the acid−base neutralization reactions, as has been demonstrated for carbonic acid.[35] Here we have applied these now well-established free-energy−reactivity correlation relationships to conclude that proton transfer hydrolysis/methanolysis pathway II dominates for 7HQ in water/methanol solvent mixtures. For this, we use the reported free-energy−reactivity relationship,[35] and use experimentally determined rate constants as input to derive values for ΔpK_a = pK_a(donor) − pK_a(protonated acceptor) (Tables 1 and 2, and Figure 4).

Table 1 summarizes our findings using literature values for 7HQ in either aqueous or methanol solution.[28,29,33] Table 2 shows the resulting values for ΔpK_a = pK_a(donor) − pK_a(protonated acceptor) from the time constants derived from the kinetic analysis of the ultrafast UV/IR pump−probe measurements on 7HQ in the deuterated water/methanol mixtures (Supporting Information), using the Marcus BEBO free-energy−reactivity relationship. For 7HQ in neat D_2O, we have derived a value for the ΔpK_a value from the reported value obtained by Bardez in neat H_2O,[28] assuming a regular H/D kinetic isotope effect (i.e., $\tau_{D_2O} = 1.4\tau_{H_2O}$). Figure 4 depicts our findings on 7HQ dissolved in neat CD_3OD as well as the X_{D_2O}:X_{CD_3OD} solvent mixtures using our femtosecond UV/IR pump−probe measurements for the overall N* ⇆ ΔZ* proton transfer reaction as well as for the C* ⇆ ΔZ* and A* ⇆ ΔZ* steps in neat CD_3OD.[33] For comparison, we also have added previously reported results by other research groups obtained with time-correlated single-photon counting (TCSPC) measurements.[28,29] It follows that the measurements performed in H_2O, in CH_3OH, and in CD_3OD all follow the same free-energy−reactivity correlation, provided that the N* ⇆ ΔZ* reaction underlies a change in value of ΔpK_a = pK_a(donor) − pK_a(protonated acceptor) by increasing by about 1.2−1.3 units when going from H_2O to CH_3OH (or, equivalently, from D_2O to CD_3OD) as the solvent. This result strongly points to the quinoline unit dominating the overall proton transfer dynamics for the N* → Z* conversion because for the naphthol unit a shift of 3−5 units is expected.[41−43] Hence we conclude that our experimental results are indicative of a proton transport mechanism via N* → C* → Z* pathway II (i.e., an inverse proton transfer mechanism by hydroxide/

DOI: 10.1021/jacs.9b03471
J. Am. Chem. Soc. 2019, 141, 14581−14592

methoxide transfer). An additional increase in magnitude of 0.3−0.5 unit for ΔpK_a = pK_a(donor) − pK_a(protonated acceptor) occurs when one exchanges CH_3OH for CD_3OD.[34] Because we do not observe any irregularities in the free-energy−reactivity correlation for 7HQ in the water/methanol mixtures, we derive that at the level of our ensemble-averaged observations of the proton/deuteron transfer reaction dynamics, no preference can be concluded for proton transfer via either water or methanol.

Figure 5 shows the derived effective ΔpK_a values for the D_2O/CD_3OD solvent mixtures as a function of molar fraction

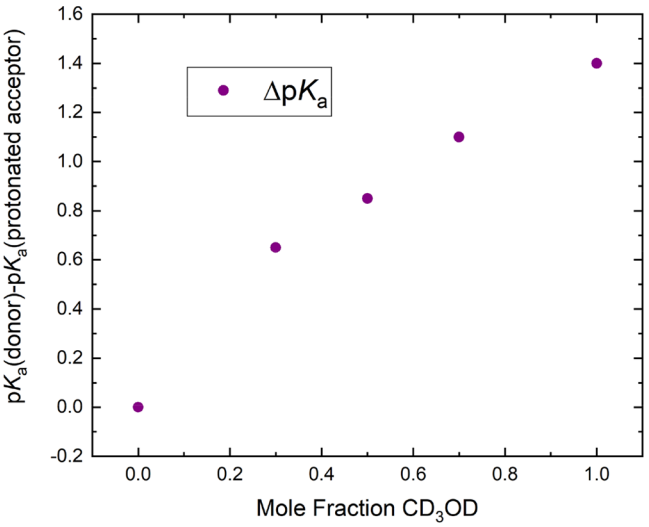

Figure 5. Effective ΔpK_a values derived from the reaction kinetics of 7HQ in D_2O/CD_3OD solvent mixtures, using the free-energy−reactivity relationship as defined by the Marcus BEBO model (shown in Figure 4b).

of CD_3OD. From ΔpK_a = pK_a(donor) − pK_a(protonated acceptor), we are able to assess the reactivity of N* as a deuteron acceptor (when ΔpK_a = pK_a(D_2O or CD_3OD) − pK_a(C*)) or of N* as a deuteron donor (when ΔpK_a = pK_a(N*) − pK_a(D_3O^+ or $CD_3OD_2^+$)). Results are shown in Table 2. We use reported values for the autoprotolysis constants of H_2O, D_2O, and CH_3OH as well as for water/methanol mixtures[43,49−51] to specify the acidities of D_3O^+ or $CD_3OD_2^+$ and of D_2O/CD_3OD in the deuterated water/methanol mixtures. Here $pK_a(D_3O^+)$ = $pK_a(CD_3OD_2^+)$ = 0 (i.e., we use the acidity value of $D_3O^+/CD_3OD_2^+$ without taking into account the self-concentration of water or methanol[36,52]). From these reported values, we also learn that the acidity of the solvent molecules in the deuterated solvent mixtures remains close to that of neat D_2O, down to molar fractions of D_2O of as low as 0.2, and significantly changes—albeit modestly in absolute magnitude—only when reaching the neat CD_3OD case. For either proton transfer scenario, as shown in Figure 1, the resulting derived changes for the pK_a* value for either N* (as the deuteron donor in the N* → A* step in pathway I) or C* (as the deuteron acceptor in the N* → C* step in pathway II) as a function of solvent composition remain modest in magnitude. The overall change of only 1.4 pK_a units when going from D_2O to CD_3OD as a solvent is compatible only with the protonated nitrogen base character of C* and not with the naphthol acid character of N*. We conclude that the almost linear dependence of ΔpK_a as a function of the molar fraction of CD_3OD, with a slope consistent for proton abstraction by the quinoline moiety, reflects a rate-determining N* → C* reaction step in the N* → C* → Z* dominating pathway for the whole range of D_2O/CD_3OD solvent mixtures.

2.3. Microsolvation around 7HQ. To investigate further the underlying microscopic mechanisms of proton transport between donating and accepting groups of 7HQ in water/methanol mixtures, we have performed equilibrium molecular dynamics (MD) simulations to investigate the microscopic solvation of 7HQ, adiabatic MD calculations using a TD-DFT molecular mechanics (MM) approach to identify the propensity of particular ultrafast protonation events of 7HQ in the S_1-state, and ab initio molecular dynamics (AIMD) simulations to obtain key insight into the proton transport along a solvent bridge, following the initial proton transfer between 7HQ and the solvent. In this Section we first investigate the distribution of water and methanol around 7HQ.

The local distribution of H_2O and CH_3OH molecules in direct proximity of the 7HQ chromophore differs significantly from the homogeneous distribution. As a consequence, the C* or A* formation, the migration of intermediate solvent ions, and the formation of the N* state might occur at local densities and mixing ratios that are different from the bulk. To analyze the extent of this effect, we computed radial pair distribution functions (RDFs) that inform about radial density variations relative to the bulk from AIMD simulations of N in the electronic ground state. The RDFs in Figure 6a indicate a slightly locally increased methanol density for both mixing

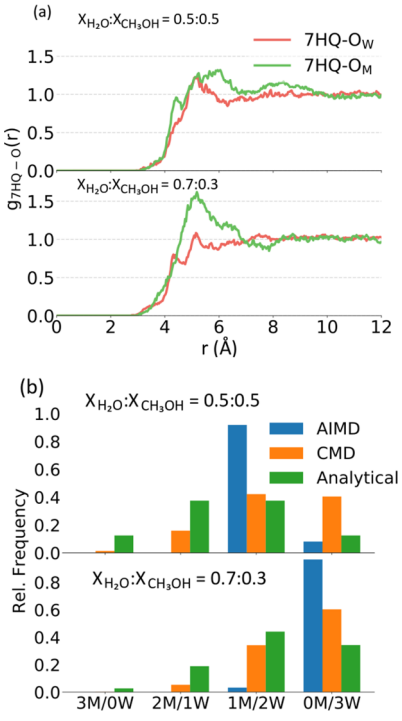

Figure 6. (a) Radial pair distribution functions $g_{7HQ-O}(r)$ (RDFs) of water (O_W) and methanol (O_M) oxygen atoms and the center of mass of 7HQ. (b) Histograms of the solvent wire composition for BLYP ab initio MD simulations (AIMD), classical MD simulations (CMD), and the analytical distribution arising from counting the various combinations of finding three methanol and zero water molecules (3*M*/0W) etc. in the solvent wire for the given molar ratios (analytical).

DOI: 10.1021/jacs.9b03471
J. Am. Chem. Soc. 2019, 141, 14581−14592

ratios that extends up to 8−10 Å from the 7HQ center of mass. This effect is more pronounced for the X_{H_2O}:X_{CH_3OH} = 0.7:0.3 solution, indicating that larger solvation-induced changes occur in this case to accommodate 7HQ in the more polar solvent environment. By contrast, partial density variations of water molecules are much less pronounced. The most significant feature in the RDFs of water is seen in the case of the X_{H_2O}:X_{CH_3OH} = 0.5:0.5 solutions. Here, the RDF between water oxygen atoms and the 7HQ center indicates a slightly increased density, which can be explained by hydrogen bonding of water molecules to the 7HQ hydroxyl moiety. To conclude the RDF analysis, the solvation of 7HQ alters the spatial distribution of solvent molecules, especially of methanol molecules; however, the effect is rather moderate. This can be seen by comparing the "local" mixing ratios as calculated from the cumulative number of oxygen atoms up to a radius of 7 Å from 7HQ. The resulting values of 46:54 and 64:36 show little deviation from the overall bulk ratio of X_{H_2O}:X_{CH_3OH}= 0.50:0.50 and 0.70:0.30 simulations, respectively.

Although this site-unspecific microsolvation is not expected to significantly affect the migration of solvent ions in proximity to the chromophore, 7HQ is able to accept and donate hydrogen bonds at its photoacidic and photobasic moieties, which might alter the solvation structure more site specifically. Most importantly, the well-defined separation of these groups allows for the formation of stable hydrogen-bonded chains of solvent molecules. It has been previously shown by us that "solvent wires" which are comprised of three water molecules are particularly stable over several tens of picoseconds.[53] Hence, these configurations might serve as a potential channel for a subpicosecond tautomerization reaction. In this case, the system would be in a resting state until a solvent wire forms at which point the tautomerization reaction would take place on a subpicosecond time scale, involving the concurrent transfer of all protons within the wire.[22] For this reason, information regarding to what extent these wires are already present in the ground state might provide important clues about whether this ultrafast mechanism might play a role at all in the case of more complex solutions than neat water, such as the current water/methanol mixtures. To this end, we analyzed ab initio and classical MD trajectories of N and investigated the presence of three-membered solvent wires. As shown in Table 3, wires are

Table 3. Average Percentages of the Formation of Solvent Wires for BLYP Ab Initio (AIMD) and Classical MD (CMD) Simulations for Two X_{H_2O}:X_{CH_3OH} Molar Ratios

	0:5:0:5	0.7:0.3
AIMD	17%	9%
CMD	7%	7%

formed in 7% of the simulation time in the case of the classical MD simulations, and 9−17% in the case of the AIMD simulations. The discrepancy between the two simulation approaches is likely due to imperfect sampling in the case of the AIMD simulations as converged statistics require simulations in the nanosecond regime. Besides the existence of solvent wires, it is compelling to ask whether these configurations are preferably composed of a specific solvent type (i.e., either water or methanol) or whether the distribution of methanol versus water molecules reflects the overall bulk mixing ratio. To answer this, we computed the distribution of water and methanol molecules within the wire, shown in Figure 6b, and compared it to the distribution one would expect by merely counting the various possibilities to form wires of a specific type. As becomes apparent, there is a clear preference for water molecules over methanol molecules to be in the solvent wire than one would expect from plain statistics. Most of the wires consist either of two or three water molecules, whereas wires containing two or three methanol play only a minor role.

Apart from the solvation structure in vicinity to the chromophore, the charge migration crucially depends on the hydrogen-bonding network between solvent molecules. One obvious difference between water and methanol is that the latter has one hydrogen bonding donor site less. Therefore, the resulting network will exhibit fewer branches the more methanol molecules are present in the solution. Moreover, the higher the number of methanol molecules relative to water molecules becomes, the lower the density will be (cf. $\rho(H_2O)$ = 0.997 g/mL; $\rho(CH_3OH)$ = 0.791 g/ml at T = 298 K and p = 1 atm.).

For a comparison of the density differences for the two mixing ratios, see the RDFs between water and methanol oxygen atoms and all solvent oxygen atoms, respectively, in Figure 7. It can be seen that only the first solvation shell differs,

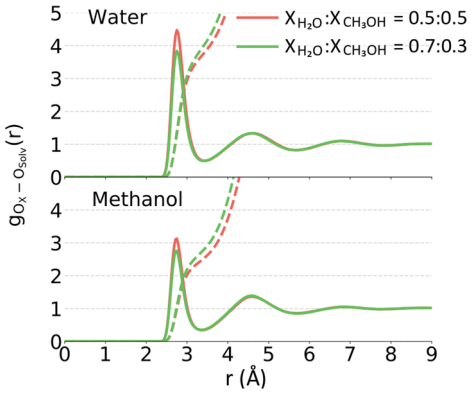

Figure 7. Radial pair distribution functions between oxygen atoms of a specific solvent type (water or methanol) and all the solvent oxygen atoms based on BLYP AIMD simulations in the electronic ground state.

whereas the remaining part of the RDF is almost identical for the two mixing ratios. The number of particles in the first solvation shell, as measured from r = 0 Å until the first minimum, is 3.7 and 4.0 for water and 2.4 and 2.6 for methanol for the X_{H_2O}:X_{CH_3OH} = 0.5:0.5 and 0.7:0.3 mixtures, respectively. It is clear, that the lower coordination number in the case of the X_{H_2O}:X_{CH_3OH} = 0.5:0.5 solutions is a consequence of the lower density. Interestingly, in the case of methanol there is a pronounced difference between the ideal coordination number of 3 and the actual coordination number observed in the MD.

Summarizing this Section: Microsolvation around 7HQ, in particular along the solvent bridge connecting the OH and N moieties, appears to show a bias to a larger number of water molecules than the statistical value given the X_{H_2O}:X_{CH_3OH} molar fractions used, even though the actual numbers depend on using either ab initio molecular dynamics (AIMD) or classical molecular dynamics (CMD) routines to determine

DOI: 10.1021/jacs.9b03471
J. Am. Chem. Soc. 2019, 141, 14581−14592

this. For the X_{H_2O}:X_{CH_3OH} mixtures investigated here, 0.5:0.5 and 0.7:0.3, the dominant configurations involve two or three water molecules, with ones consisting of methanol only playing a minor role. From our simulations we deduce that solvent bridges with full hydrogen bonds ("solvent wires") are only a minor part (7−17%) for the X_{H_2O}:X_{CH_3OH} = 0.5:0.5 and 0.7:0.3 molar fraction ratios. Hence the most typical solvent bridge configurations involve two to three water molecules with partially broken hydrogen bonds. Further details are provided in the SI.

2.4. Primary Proton Transfer Events upon Photoexcitation of 7HQ. To investigate the mechanism of N* to Z* conversion, we carried out first-principles adiabatic MD simulations of the fully solvated 7HQ in the first electronically excited state, employing TD-DFT. The main focus was on whether the reaction proceeds concertedly via a solvent wire or sequentially in a von-Grotthuss-type hopping mechanism. In the case of a sequential reaction, there are two further possibilities, namely H_3O^+/$MeOH_2^+$ or OH^-/CH_3O^- transport. For this reason, we prepared the system in two initial conditions that were based on AIMD snapshots of N in the ground state: (I.) C* with a hydrogen bonded OH^-/CH_3O^- at the nitrogen site, and (II.) A* with an H_3O^+ molecule hydrogen bonded to the A*−O^- site (cf. Figure 8). Moreover,

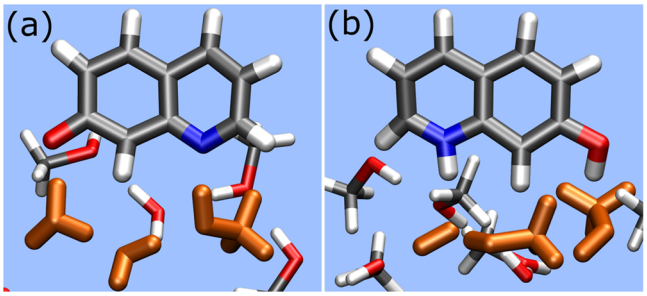

Figure 8. TD-DFT MD snapshots of (a) A* and (b) C* with surrounding solvent molecules. Molecules forming the wire are shown in orange. Only a limited number of QM atoms are shown for simplicity.

to allow for the possibility of a concerted reaction, all of the selected initial configurations exhibited a solvent wire which connected the photobasic and photoacidic sites of 7HQ. The system was propagated adiabatically on the excited-state potential energy surface for the duration of about 1 ps, while the migration of the excess charge was followed. This approach allows us to assess the temporal stability of C* and A* protonation states inside a realistic solvent environment and helps to address the question which of the possible reaction pathways is the most likely.

The simulations reveal that for most trajectories with C* as the initial state, no back transfer of the proton to the adjacent negatively charged solvent ion was observed, that would lead to the formation of the neutral N* form. Instead, the C* form remained stable over the course of these simulations and proton transfer reactions were only observed within the solvent resulting in the migration of a negatively charged solvent ion. In contrast, the proton was transferred back to the basic 7HQ oxygen atom already within the first 200 fs for trajectories if the initial state was A*. For one of the A* trajectories, we observed the transient formation of C*, that was formed after back-protonation of the 7HQ hydroxyl group. Hence, an anionic charge transfer through the solvent (i.e., based on OH^- and CH_3O^- ions) is favored, whereas the cationic variant, featuring H_3O^+ or $CH_3OH_2^+$ species, is clearly disfavored. Although our MD simulations yield a consistent picture with our experimental results, we emphasize here that significantly longer MD simulations are necessary to unequivocally assess whether there exists a pathway for a concerted transfer.

2.5. Charge Migration through the Water/Methanol Solvent Bridges. To follow the picosecond dynamics of the negative solvent ion (OH^-/CH_3O^-) beyond the ultrafast time scales accessible by the TD-DFT MD simulations, we carried out further AIMD simulations by employing the revPBE0 hybrid functional and D3 dispersion corrections. The goal of our simulations was to trace the charge migration through the solvent in close proximity to the 7HQ chromophore and to elucidate the role of the hydrogen-bonding network of the solvent on the charge migration mechanism. For this, the definition of asymmetry parameter δ for proton location along a hydrogen bond between donating and accepting sites is shown in Figure 9. Here, 7HQ was modeled by classical force

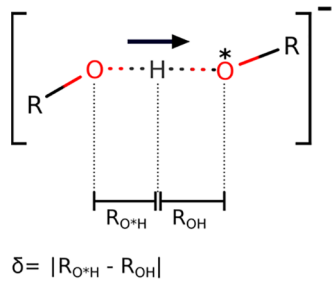

Figure 9. Definition of asymmetry parameter δ for proton location along a hydrogen between donating and accepting sites, as used to determine the average number of donating hydrogen bonds along the solvent bridge as a function of δ.

field potentials, where we reparametrized the 7HQ partial charges with a restrained electrostatic potential fit using the S_1 electron density as a reference. This treatment implicitly assumes successful acid−base dissociation (i.e., no back-donation to the solvent occurs after the protonation of the nitrogen site). After a short equilibration phase, the charge migration was simulated for 10 ps starting from five different initial conditions.

The MD trajectories reveal that the negative charge (i.e., CH_3O^- or OH^-) migrates through the solution with the participation of both methanol and water molecules. Table 4 presents the averaged occurrences of all possible partial reactions. Here, a pronounced difference between the two mixing ratios is observed: in the case of the X_{H_2O}:X_{CH_3OH} =

Table 4. Average Occurrences of Distinct Transfer Reactions in Simulations Derived for Two X_{H_2O}:X_{CH_3OH} Molar Ratios

transfer reaction	average count for X_{H_2O}:X_{CH_3OH} = 0.5:0.5	average count for X_{H_2O}:X_{CH_3OH} = 0.7:0.3
$H_2O + OH^- \rightarrow OH^- + H_2O$	0.5	9
$MeOH + MeO^- \rightarrow MeO^- + MeOH$	5	0.3
$MeO^- + H_2O \rightarrow MeOH + OH^-$	3	3
$MeOH + OH^- \rightarrow MeO^- + H_2O$	4	1.3

DOI: 10.1021/jacs.9b03471
J. Am. Chem. Soc. 2019, 141, 14581−14592

0.5:0.5 solutions, the charge migrates dominantly between methanol or methoxide species, whereas for the X_{H_2O}:X_{CH_3OH} = 0.7:0.3 solutions, charge transfer is almost exclusively observed between water molecules. Therefore, at higher water concentrations the charge migrates preferentially via water molecules whereas methanol species play only a minor role.

To elucidate the underlying transfer mechanism, the hydrogen bonding configurations of the reacting species at various times during the transfer were analyzed. The left panel of Figure 10 shows the average number of hydrogen bonds for

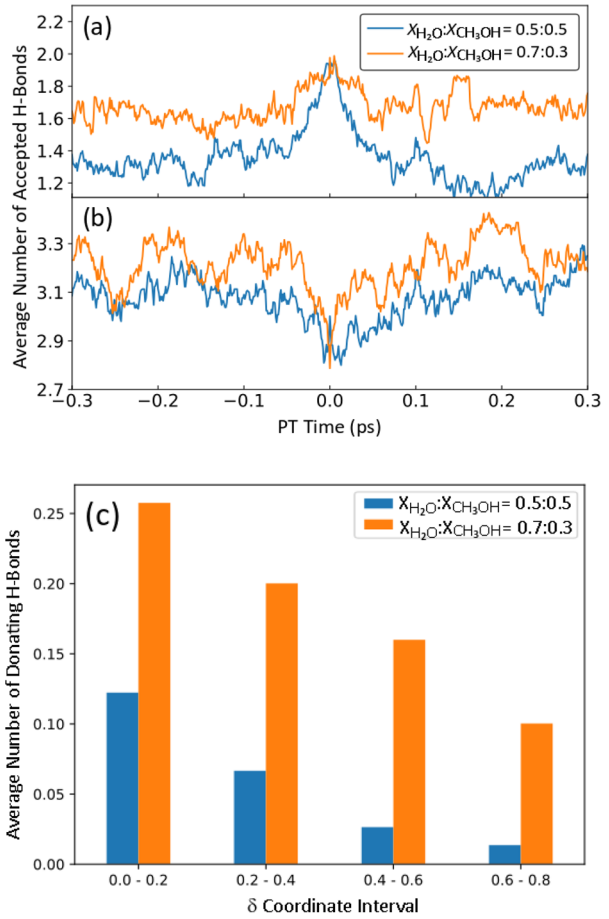

Figure 10. Average number of accepted hydrogen bonds of (a) the proton-donating solvent molecule and (b) the solvent ion (OH^- or CH_3O^-) as a function of the proton transfer time. The time origin is the time when the proton is symmetrically shared between donating and accepting oxygen atoms. Note that the proton-donating solvent molecule and the solvent ion definitions interchange their respective roles for times >0. (c) Average number of donating hydrogen bonds of the OH^- ion as a function of the asymmetry parameter δ (as defined in Figure 9) for the two mixing ratios. A small δ value indicates structures close to the transition state, where the proton is symmetrically shared between the two oxygen atoms, whereas larger values indicate structures close to free-energy minima.

the proton-donating solvent molecule (Figure 10a) and the solvent ion (Figure 10b), respectively. It was not distinguished as to whether the solvent ion was methoxide or hydroxide. It can be seen that because of the lower density in the case of the X_{H_2O}:X_{CH_3OH} = 0.5:0.5 mixture, the number of accepting hydrogen bonds is reduced by about 0.2. However, when the proton is shared between the two solvent molecules (i.e., for structures close to the transition state), the number of hydrogen bonds is the same for both water/methanol ratios. Therefore, the simulations strongly support that the same underlying transfer mechanism exists in both cases. During the transfer, the number of accepted hydrogen bonds at the donor molecule increases to its ideal number, 2. On the other hand, the number of accepting hydrogen bonds at the solvent ion drops on average to 2.9 at the transition state. This has important consequences. In the case of the X_{H_2O}:X_{CH_3OH} = 0.5:0.5 solution, larger changes in the hydrogen-bonding network are required at the donor molecule because the number of accepting hydrogen bonds is less because of the lower density. The situation is reversed for the X_{H_2O}:X_{CH_3OH} = 0.7:0.3 mixtures. Here, the changes in the hydrogen bonding configuration are most pronounced at the solvent ion. This is because at higher water concentrations there is an increasing number of hypercoordinated methanolate or hydroxide ions (i.e., structures that accept four hydrogen bonds). Consequently, the coordination number difference between solvent ions in their minimum free energy and their transition-state configuration also increases. Therefore, our simulations reveal that two mechanistically counteracting effects are occurring when altering the water/methanol ratio. Notably, the changes in hydrogen bonding are larger in the case of the X_{H_2O}:X_{CH_3OH} = 0.5:0.5 solutions, which may be one reason for the lower conductivities in this case.

Our results are in line with what one would expect from the presolvation concept proposed by Tuckerman et al.[23,24] However, these studies pointed out that in the dynamical hypercoordination mechanism of hydroxide ion migration in water, a donating hydrogen bond of the hydroxide ion plays an important role. To investigate this for our water/methanol mixtures, we computed the average number of donating hydrogen bonds of the hydroxide ion for different stages of the reaction. Note that methoxide lacks the possibility to donate a hydrogen bond. The results are shown in Figure 10c. It can be seen that with increasing water concentration the average number of hydrogen bonds increases drastically. The relative frequency more than doubles when going from X_{H_2O}:X_{CH_3OH} = 0.5:0.5 to 0.7:0.3 molar fraction ratios. Moreover, it increases significantly for structures that share the proton symmetrically (low δ values), but the relative frequencies of a donating hydrogen bond are still low for both ratios. Hence, the donating hydrogen bond of the hydroxide ion plays only a minor role in the case of the investigated concentration ratios and therefore is not a necessary condition for the charge transfer in water/methanol mixtures at the concentrations investigated here.

3. CONCLUSIONS

We have studied, in a combined femtosecond UV/IR pump–probe spectroscopic and ab initio molecular dynamics study, proton exchange dynamics between the proton-donating naphthol OH group and the proton-accepting quinoline N-moiety of bifunctional photoacid 7HQ in water/methanol solvent mixtures. We can exclude the major role of the sequential proton excess (protonated water/methanol) transport mechanism (pathway I in Figure 1b) because our findings on solvent-composition-dependent changes in reaction rates are not compatible with those with respect to the acidities of the proton-donating naphthol unit in 7HQ. We can also

DOI: 10.1021/jacs.9b03471
J. Am. Chem. Soc. 2019, 141, 14581−14592

exclude that direct "concerted" proton transfer occurs for a fraction of 7HQ (pathway III in Figure 1b), as even though for about 10% of the ensemble a full hydrogen-bonded solvent network exists that connects proton-donating and -accepting sides upon electronic excitation, and our detailed kinetic analysis of the transient UV/IR pump−probe spectra does not show any significant early time components that would support a transfer event within the lifetimes of this "solvent wire" (that will not extend beyond several picoseconds[54,55]). One may argue that a direct proton exchange occurs on ultrafast (femtosecond/few picosecond) time scales only when an intact hydrogen-bonded network is formed, and the ensemble-averaged reaction time constants of tens to hundreds of picoseconds are merely a result of long waiting times between the breaking and formation of these "solvent wires". Both free-energy−reactivity correlations (complying with values observed for proton transfer in the bulk solvent) and trajectories resulting from the ab initio molecular dynamics simulations point to a sequential transfer mechanism, with proton abstraction from the solvent event being the first as well as the rate-determining step. Hence, we conclude that proton exchange between the proton-donating naphthol OH group and the proton-accepting quinoline N-moiety of the bifunctional photoacid 7HQ, linked together by a water/methanol solvent bridge, occurs by a sequential hydroxide/methoxide transport mechanism taking place on ensemble-averaged time scales of tens to hundreds of picoseconds (pathway II in Figure 1b).

The observation that charge migration along a preformed solvent bridge at the hydrophobic 7HQ−solvent interface proceeds in a stepwise manner has direct implications for the understanding of charge migration along other hydrophobic interfaces, such as in proton channels, where there is still an ongoing debate as to whether concerted proton transfer is the reason for the high efficiencies of biological proton channels. Free-energy−reactivity correlations show that for all X_{H_2O}:X_{CH_3OH} mixing ratios bulk acidities (pK_a values) follow general trends in solvent polarity, strongly advocating for further studies of the applicability of such correlations between acidities and reaction time scales for proton transport near apolar regions, as well as polar or ionic functionalities within transmembrane proteins and hydrogen fuel cells. In this context, our results may be of use in both accurate pK_a value determination[56,57] under solvent conditions clearly different from those of bulk water[58] and detailed studies of particular proton-donating or -accepting groups in proton-pump transmembrane proteins[8,59−61] or proton-exchange membrane fuel cells.[62−64] Finally, our combined experimental and theoretical study shows the equal importance of hydrolysis/methanolysis as possible alternative pathway to the more intensively studied protolysis pathway for acid−base neutralization in protic solvents as originally formulated by Eigen.

■ ASSOCIATED CONTENT

Supporting Information

The Supporting Information is available free of charge on the ACS Publications website at DOI: 10.1021/jacs.9b03471.

Experimental details, computational details, principal component analysis of 7HQ UV/IR pump−probe data including supplementary figures S1−S4, supplementary table S1, and supplementary references S1−S38 (PDF)

■ AUTHOR INFORMATION

Corresponding Authors

*E-mail: nibberin@mbi-berlin.de.
*E-mail: daniel.sebastiani@chemie.uni-halle.de.

ORCID

Oleg Kornilov: 0000-0002-3343-2614
Erik T. J. Nibbering: 0000-0001-5874-8052

Notes

The authors declare no competing financial interest.

■ ACKNOWLEDGMENTS

This work has benefitted from financial support by the German Science Foundation (project no. NI 492/13-1/SE 1008/11-1) and the European Research Council (ERC) under the European Union's Horizon 2020 research and innovation programme (ERC grant agreement no. 788704; E.T.J.N.). F.H. cordially thanks the Fonds der Chemischen Industrie for a Kekulé fellowship. A.R. cordially thanks the European Commission for an Erasmus+ Trainee Fellowship. We are grateful for stimulating discussions with Prof. Dr. Ehud Pines and Dr. Dina Pines. E.T.J.N. dedicates this work to the memory of Prof. Dr. Dan Huppert, pioneer of ultrafast photoacid spectroscopy.

■ REFERENCES

(1) Eigen, M.; Kruse, W.; Maass, G.; DeMaeyer, L. Rate Constants of Protolytic Reactions in Aqueous Solution. *Prog. React. Kinet.* **1964**, *2*, 285.
(2) Weller, A. Fast Reactions of Excited Molecules. *Prog. React. Kinet.* **1961**, *1*, 187−213.
(3) Eigen, M. Proton Transfer, Acid-Base Catalysis, and Enzymatic Hydrolysis. Part 1: Elementary Processes. *Angew. Chem., Int. Ed. Engl.* **1964**, *3*, 1−19.
(4) Bell, R. P. *The Proton in Chemistry*, 2nd ed.; Chapman and Hall: London, 1973.
(5) Stillinger, F. H. Proton Transfer Reactions and Kinetics in Water. In *Theoretical Chemistry: Advances and Perspectives*; Eyring, H., Henderson, D., Eds.; Academic Press: New York, 1978; Vol. 3, pp 177−234.
(6) Hedstrom, L. Serine Protease Mechanism and Specificity. *Chem. Rev.* **2002**, *102*, 4501−4523.
(7) Lee, H. J.; Svahn, E.; Swanson, J. M. J.; Lepp, H.; Voth, G. A.; Brzezinski, P.; Gennis, R. B. Intricate Role of Water in Proton Transport through Cytochrome C Oxidase. *J. Am. Chem. Soc.* **2010**, *132*, 16225−16239.
(8) Freier, E.; Wolf, S.; Gerwert, K. Proton Transfer Via a Transient Linear Water-Molecule Chain in a Membrane Protein. *Proc. Natl. Acad. Sci. U. S. A.* **2011**, *108*, 11435−11439.
(9) Salna, B.; Benabbas, A.; Sage, J. T.; van Thor, J.; Champion, P. M. Wide-Dynamic-Range Kinetic Investigations of Deep Proton Tunnelling in Proteins. *Nat. Chem.* **2016**, *8*, 874−880.
(10) Mohammed, O. F.; Pines, D.; Dreyer, J.; Pines, E.; Nibbering, E. T. J. Sequential Proton Transfer through Water Bridges in Acid-Base Reactions. *Science* **2005**, *310*, 83−86.
(11) Mohammed, O. F.; Pines, D.; Nibbering, E. T. J.; Pines, E. Base-Induced Solvent Switches in Acid-Base Reactions. *Angew. Chem., Int. Ed.* **2007**, *46*, 1458−1469.
(12) Mohammed, O. F.; Pines, D.; Pines, E.; Nibbering, E. T. J. Aqueous Bimolecular Proton Transfer in Acid-Base Neutralization. *Chem. Phys.* **2007**, *341*, 240−257.
(13) Siwick, B. J.; Bakker, H. J. On the Role of Water in Intermolecular Proton-Transfer Reactions. *J. Am. Chem. Soc.* **2007**, *129*, 13412−13420.
(14) Thomas, V.; Rivard, U.; Maurer, P.; Bruhacs, A.; Siwick, B. J.; Iftimie, R. Concerted and Sequential Proton Transfer Mechanisms in

Water-Separated Acid-Base Encounter Pairs. *J. Phys. Chem. Lett.* **2012**, *3*, 2633−2637.
(15) Rivard, U.; Thomas, V.; Bruhacs, A.; Siwick, B.; Iftimie, R. Donor-Bridge-Acceptor Proton Transfer in Aqueous Solution. *J. Phys. Chem. Lett.* **2014**, *5*, 3200−3205.
(16) Marx, D.; Tuckerman, M. E.; Hutter, J.; Parrinello, M. The Nature of the Hydrated Excess Proton in Water. *Nature* **1999**, *397*, 601−4.
(17) Vuilleumier, R.; Borgis, D. Transport and Spectroscopy of the Hydrated Proton: A Molecular Dynamics Study. *J. Chem. Phys.* **1999**, *111*, 4251−4266.
(18) Schmitt, U. W.; Voth, G. A. The Computer Simulation of Proton Transport in Water. *J. Chem. Phys.* **1999**, *111*, 9361−9381.
(19) Marx, D. Proton Transfer 200 Years after von Grotthuss: Insights from Ab Initio Simulations. *ChemPhysChem* **2006**, *7*, 1848−1870.
(20) Xu, J.; Zhang, Y.; Voth, G. A. Infrared Spectrum of the Hydrated Proton in Water. *J. Phys. Chem. Lett.* **2011**, *2*, 81−86.
(21) Kulig, W.; Agmon, N. A 'Clusters-in-Liquid' Method for Calculating Infrared Spectra Identifies the Proton-Transfer Mode in Acidic Aqueous Solutions. *Nat. Chem.* **2013**, *5*, 29−35.
(22) Hassanali, A.; Giberti, F.; Cuny, J.; Kühne, T. D.; Parrinello, M. Proton Transfer through the Water Gossamer. *Proc. Natl. Acad. Sci. U. S. A.* **2013**, *110*, 13723−13728.
(23) Tuckerman, M. E.; Marx, D.; Parrinello, M. The Nature and Transport Mechanism of Hydrated Hydroxide Ions in Aqueous Solution. *Nature* **2002**, *417*, 925−929.
(24) Marx, D.; Chandra, A.; Tuckerman, M. E. Aqueous Basic Solutions: Hydroxide Solvation, Structural Diffusion, and Comparison to the Hydrated Proton. *Chem. Rev.* **2010**, *110*, 2174−2216.
(25) Chen, M.; Zheng, L.; Santra, B.; Ko, H.-Y.; DiStasio, R. A., Jr.; Klein, M. L.; Car, R.; Wu, X. Hydroxide Diffuses Slower Than Hydronium in Water Because Its Solvated Structure Inhibits Correlated Proton Transfer. *Nat. Chem.* **2018**, *10*, 413−419.
(26) Ditkovich, J.; Mukra, T.; Pines, D.; Huppert, D.; Pines, E. Bifunctional Photoacids: Remote Protonation Affecting Chemical Reactivity. *J. Phys. Chem. B* **2015**, *119*, 2690−2701.
(27) Mason, S. F.; Philp, J.; Smith, B. E. Prototropic Equilibria of Electronically Excited Molecules. 2. 3-, 6-, and 7-Hydroxyquinoline. *J. Chem. Soc. A* **1968**, 3051−3056.
(28) Bardez, E. Excited-State Proton Transfer in Bifunctional Compounds. *Isr. J. Chem.* **1999**, *39*, 319−332.
(29) Konijnenberg, J.; Ekelmans, G. B.; Huizer, A. H.; Varma, C. Mechanism and Solvent Dependence of the Solvent-Catalyzed Pseudo-Intramolecular Proton-Transfer of 7-Hydroxyquinoline in the 1st Electronically Excited Singlet-State and in the Ground-State of Its Tautomer. *J. Chem. Soc., Faraday Trans. 2* **1989**, *85*, 39−51.
(30) Chou, P.-T.; Wei, C.-Y.; Wang, C.-R. C.; Hung, F.-T.; Chang, C.-P. Proton-Transfer Tautomerism of 7-Hydroxyquinolines Mediated by Hydrogen-Bonded Complexes. *J. Phys. Chem. A* **1999**, *103*, 1939−1949.
(31) Kwon, O. H.; Lee, Y. S.; Yoo, B. K.; Jang, D. J. Excited-State Triple Proton Transfer of 7-Hydroxyquinoline Along a Hydrogen-Bonded Alcohol Chain: Vibrationally Assisted Proton Tunneling. *Angew. Chem., Int. Ed.* **2006**, *45*, 415−419.
(32) Kwon, O.-H.; Mohammed, O. F. Water-Wire Catalysis in Photoinduced Acid-Base Reactions. *Phys. Chem. Chem. Phys.* **2012**, *14*, 8974−8980.
(33) Hoffmann, F.; Ekimova, M.; Bekçioğlu-Neff, G.; Nibbering, E. T. J.; Sebastiani, D. Combined Experimental and Theoretical Study of the Transient IR Spectroscopy of 7-Hydroxyquinoline in the First Electronically Excited Singlet State. *J. Phys. Chem. A* **2016**, *120*, 9378−9389.
(34) Pines, E. The Kinetic Isotope Effect in the Photo-Dissociation Reaction of Excited-State Acids in Aqueous Solutions. In *Isotope Effects in Chemistry and Biology*; Kohen, A., Limbach, H.-H., Eds.; CRC Taylor & Francis: Boca Raton, FL, 2006; pp 451−464.
(35) Adamczyk, K.; Prémont-Schwarz, M.; Pines, D.; Pines, E.; Nibbering, E. T. J. Real-Time Observation of Carbonic Acid Formation in Aqueous Solution. *Science* **2009**, *326*, 1690−1694.
(36) Munitz, N.; Avital, Y.; Pines, D.; Nibbering, E. T. J.; Pines, E. Cation-Enhanced Deprotonation of Water by a Strong Photobase. *Isr. J. Chem.* **2009**, *49*, 261−272.
(37) Prémont-Schwarz, M.; Barak, T.; Pines, D.; Nibbering, E. T. J.; Pines, E. Ultrafast Excited-State Proton-Transfer Reaction of 1-Naphthol-3,6-Disulfonate and Several 5-Substituted 1-Naphthol Derivatives. *J. Phys. Chem. B* **2013**, *117*, 4594−4603.
(38) Rini, M.; Kummrow, A.; Dreyer, J.; Nibbering, E. T. J.; Elsaesser, T. Femtosecond Mid-Infrared Spectroscopy of Condensed Phase Hydrogen-Bonded Systems as a Probe of Structural Dynamics. *Faraday Discuss.* **2003**, *122*, 27−40.
(39) Mohammed, O. F.; Dreyer, J.; Magnes, B.-Z.; Pines, E.; Nibbering, E. T. J. Solvent-Dependent Photoacidity State of Pyranine Monitored by Transient Mid-Infrared Spectroscopy. *ChemPhysChem* **2005**, *6*, 625−636.
(40) Psciuk, B. T.; Prémont-Schwarz, M.; Koeppe, B.; Keinan, S.; Xiao, D.; Nibbering, E. T. J.; Batista, V. S. Correlating Photoacidity to Hydrogen-Bond Structure by Using the Local O-H Stretching Probe in Hydrogen-Bonded Complexes of Aromatic Alcohols. *J. Phys. Chem. A* **2015**, *119*, 4800−4812.
(41) Rived, F.; Roses, M.; Bosch, E. Dissociation Constants of Neutral and Charged Acids in Methyl Alcohol. The Acid Strength Resolution. *Anal. Chim. Acta* **1998**, *374*, 309−324.
(42) Rived, F.; Canals, I.; Bosch, E.; Rosés, M. Acidity in Methanol-Water. *Anal. Chim. Acta* **2001**, *439*, 315−333.
(43) Cox, B. G. *Acids and Bases: Solvent Effects on Acid-Base Strengths*; Oxford University Press: Oxford, 2013.
(44) Pines, E.; Fleming, G. R. Proton-Transfer in Mixed Water Organic-Solvent Solutions - Correlation between Rate, Equilibrium-Constant, and the Proton Free-Energy of Transfer. *J. Phys. Chem.* **1991**, *95*, 10448−10457.
(45) Spies, C.; Shomer, S.; Finkler, B.; Pines, D.; Pines, E.; Jung, G.; Huppert, D. Solvent Dependence of Excited-State Proton Transfer from Pyranine-Derived Photoacids. *Phys. Chem. Chem. Phys.* **2014**, *16*, 9104−9114.
(46) Marcus, R. A. The 2nd R. A. Robinson Memorial Lecture - Electron, Proton and Related Transfers. *Faraday Discuss. Chem. Soc.* **1982**, *74*, 7−15.
(47) Marcus, R. A. Theoretical Relations among Rate Constants Barriers and Brønsted Slopes of Chemical Reactions. *J. Phys. Chem.* **1968**, *72*, 891−899.
(48) Cohen, A. O.; Marcus, R. A. On Slope of Free Energy Plots in Chemical Kinetics. *J. Phys. Chem.* **1968**, *72*, 4249−4256.
(49) Parsons, G. H.; Rochester, C. H. Thermodynamics of Autoionization of Methanol and Water Mixtures. *J. Chem. Soc., Faraday Trans. 1* **1972**, *68*, 523−532.
(50) Gerritzen, D.; Limbach, H. H. Kinetic and Equilibrium Isotope Effects of Proton-Exchange and Autoprotolysis of Pure Methanol Studied by Dynamic NMR-Spectroscopy. *Ber. Bunsen-Ges. Phys. Chem.* **1981**, *85*, 527−535.
(51) Rondinini, S.; Longhi, P.; Mussini, P. R.; Mussini, T. Autoprotolysis Constants in Nonaqueous Solvents and Aqueous Organic-Solvent Mixtures. *Pure Appl. Chem.* **1987**, *59*, 1693−1702.
(52) Silverstein, T. P.; Heller, S. T. pK_a Values in the Undergraduate Curriculum: What Is the Real pK_a of Water? *J. Chem. Educ.* **2017**, *94*, 690−695.
(53) Bekçioğlu, G.; Allolio, C.; Sebastiani, D. Water Wires in Aqueous Solutions from First-Principles Calculations. *J. Phys. Chem. B* **2015**, *119*, 4053−4060.
(54) Laage, D.; Stirnemann, G.; Sterpone, F.; Rey, R.; Hynes, J. T. Reorientation and Allied Dynamics in Water and Aqueous Solutions. *Annu. Rev. Phys. Chem.* **2011**, *62*, 395−416.
(55) Mazur, K.; Bonn, M.; Hunger, J. Hydrogen Bond Dynamics in Primary Alcohols: A Femtosecond Infrared Study. *J. Phys. Chem. B* **2015**, *119*, 1558−1566.

DOI: 10.1021/jacs.9b03471
J. Am. Chem. Soc. 2019, 141, 14581−14592

(56) Kelly, C. P.; Cramer, C. J.; Truhlar, D. G. Aqueous Solvation Free Energies of Ions and Ion-Water Clusters Based on an Accurate Value for the Absolute Aqueous Solvation Free Energy of the Proton. *J. Phys. Chem. B* **2006**, *110*, 16066−16081.
(57) Ho, J. M.; Coote, M. L. A Universal Approach for Continuum Solvent Pk_a Calculations: Are We There Yet? *Theor. Chem. Acc.* **2010**, *125*, 3−21.
(58) Raamat, E.; Kaupmees, K.; Ovsjannikov, G.; Trummal, A.; Kutt, A.; Saame, J.; Koppel, I.; Kaljurand, I.; Lipping, L.; Rodima, T.; Pihl, V.; Koppel, I. A.; Leito, I. Acidities of Strong Neutral Brønsted Acids in Different Media. *J. Phys. Org. Chem.* **2013**, *26*, 162−170.
(59) Bashford, D.; Gerwert, K. Electrostatic Calculations of the Pk_a Values of Ionizable Groups in Bacteriorhodopsin. *J. Mol. Biol.* **1992**, *224*, 473−486.
(60) Zscherp, C.; Schlesinger, R.; Tittor, J.; Oesterhelt, D.; Heberle, J. In Situ Determination of Transient pK_a Changes of Internal Amino Acids of Bacteriorhodopsin by Using Time-Resolved Attenuated Total Reflection Fourier-Transform Infrared Spectroscopy. *Proc. Natl. Acad. Sci. U. S. A.* **1999**, *96*, 5498−5503.
(61) Lorenz-Fonfria, V. A.; Saita, M.; Lazarova, T.; Schlesinger, R.; Heberle, J. p*H*-Sensitive Vibrational Probe Reveals a Cytoplasmic Protonated Cluster in Bacteriorhodopsin. *Proc. Natl. Acad. Sci. U. S. A.* **2017**, *114*, E10909−E10918.
(62) Hickner, M. A.; Ghassemi, H.; Kim, Y. S.; Einsla, B. R.; McGrath, J. E. Alternative Polymer Systems for Proton Exchange Membranes (PEMS). *Chem. Rev.* **2004**, *104*, 4587−4611.
(63) Higashihara, T.; Matsumoto, K.; Ueda, M. Sulfonated Aromatic Hydrocarbon Polymers as Proton Exchange Membranes for Fuel Cells. *Polymer* **2009**, *50*, 5341−5357.
(64) Sadakiyo, M.; Yamada, T.; Kitagawa, H. Hydrated Proton-Conductive Metal-Organic Frameworks. *ChemPlusChem* **2016**, *81*, 691−701.

DOI: 10.1021/jacs.9b03471
J. Am. Chem. Soc. 2019, 141, 14581−14592